

We are IntechOpen, the world's leading publisher of Open Access books Built by scientists, for scientists

6,900

Open access books available

186,000

International authors and editors

200M

Downloads

Our authors are among the

154

Countries delivered to

TOP 1%

most cited scientists

12.2%

Contributors from top 500 universities



WEB OF SCIENCE™

Selection of our books indexed in the Book Citation Index
in Web of Science™ Core Collection (BKCI)

Interested in publishing with us?
Contact book.department@intechopen.com

Numbers displayed above are based on latest data collected.
For more information visit www.intechopen.com



Review of Research on the Thermoelectric Material

ZnSb

Xin Song and Terje G. Finstad

Additional information is available at the end of the chapter

<http://dx.doi.org/10.5772/65661>

Abstract

The thermoelectric material ZnSb has been studied intensively in recent years and has shown promising features. The other zinc-antimonide compound, Zn_4Sb_3 has remarkable low thermal conductivity, but it is accompanied with phase transitions at moderate temperature and has inherent stability problems. Compared to that, ZnSb is relatively phase stable and has a relative high charge carrier mobility and Seebeck coefficient, thus yielding a decent power factor. Meanwhile, its thermal conductivity can be reduced by means of nanostructuring, thus giving a good figure of merit at moderate temperatures, 400–600 K. Many researchers have dedicated their efforts to study and improve ZnSb properties, and the figure of merit has been reported to be above one. Still, ZnSb as a thermoelectric material has features and behaviours that are not well-understood. The behaviour and properties of its intrinsic defects are not understood, but have interested researchers in recent years. This chapter intends to offer a comprehensive review on ZnSb to the readers. By combining own experiences from research on thermoelectric materials, the authors address the prospect for improving the thermoelectric properties of ZnSb and the concerns of transferring lab results to manufacturing.

Keywords: zinc antimonide, impurity band conduction, intrinsic defects, vacancies, *p*-type

1. Introduction

The thermoelectric effect in ZnSb has been known for almost two centuries. The first documented encounter can be traced back to the original work of Seebeck on thermoelectric current generation on different materials and alloy pairs in 1819–1827 [1, 2]. Quantitative measurements of the Seebeck voltage of ZnSb have been carried out by Becquerel in 1866 [3],

and thermoelectric generators using Zn-Sb alloy were fabricated for practical purposes since 1870 [4]. From the early twentieth century, many attempted to solve the crystal structure, but were barely successful [5–7], until Almin, finally, in 1948 determined the crystal structure of ZnSb together with CdSb [8]. A large interest in ZnSb followed and was benefitted by the progress on semiconductors since the 1950s. **Figure 1** shows a thermoelectric device made by ZnSb in the 1950s. It shows a solar thermoelectric generator prototype built by p -ZnSb and n -Bi₉₁Sb₉ with an overall efficiency of 0.63% [9]. Around the same time, a thermoelectric refrigerator made of n -PbTe and p -ZnSb was demonstrated in the USSR in the 1950s [10]. However, research reporting on ZnSb faded in the 1970s, and there was little improvement in terms of its efficiency. In recent years, renewed attention appeared due to a nanostructuring boom in material science, and the thermoelectric properties of ZnSb have been intensively studied and improved. There are also other energy-related applications of ZnSb actively being explored, such as electrodes for rechargeable Li-ion batteries [11], or phase change memory cells [12].

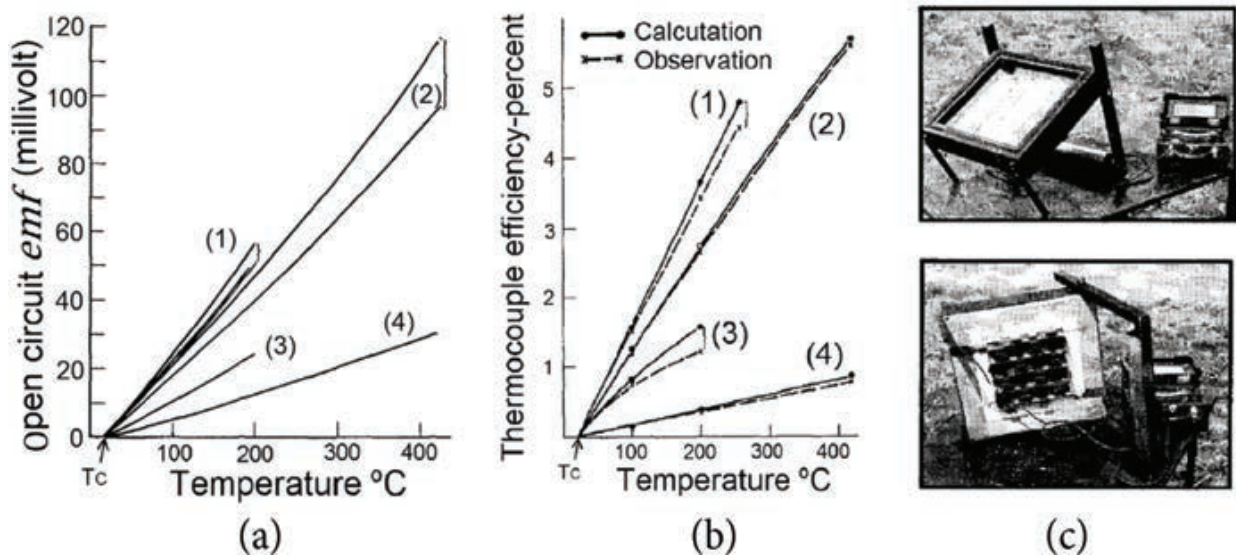


Figure 1. Solar thermoelectric generator. (Reprinted from [9], with the permission of AIP Publishing.) (a) Open circuit emf (Seebeck coefficient) as a function of temperature on ZnSb-alloys comparing with other thermal couples. Materials: (1) ZnSb (Sn, Ag, Bi)-Bi₉₁Sb₉, (2) ZnSb (Sn, Ag, Bi)-constantan, (3) Bi₉₁Sb₉Sn₅-Bi₉₁Sb₉, (4) Chromel P-constantan. (b) Thermoelectric efficiency on aforesaid materials; (c) Solar radiation thermopile contained 25 junctions built by p -ZnSb in plot (a) and (b) and n -Bi₉₁Sb₉. Above: front surface exposed to the sun; below: rear view shows the thermoelectric junctions.

Table 1 lists some reported figure of merit zT . The performance of ZnSb strongly depends on doping concentration and operation temperature. In addition, preparation-induced defects (phase impurity, oxidation and grain size) and intrinsic defects (vacancies, interstitials, clusters) influence strongly the material's performance. These need to be controlled in order to bring further progress, and in general, handling of the material has a learning curve and a detailed understanding of the material, per se, is needed.

Report year	zT	At temperature (K)	Sample	Reference
(1961)	0.6	460	Single crystal	[13]
(1964)	0.42	300	Single crystal	[14]
(1964)	0.3	300	Polycrystalline	[14]
(1966)	0.2	273	Single crystal	[15]
(2010)	0.07	373	Polycrystalline	[16]
(2010)	0.8	573	Polycrystalline	[17]
(2012)	0.9	659	Polycrystalline with Cu	[18]
(2013)	1.15	670	Polycrystalline with Ag	[19]
(2014)	0.9	635	Polycrystalline with Ag	[20]
(2014)	0.8	600	Polycrystalline with Cu	[20]
(2014)	1	630	Polycrystalline with Sn+Cd	[21]
(2014)	1.5	673	Polycrystalline with Cu	[22]
(2015)	0.8	700	Polycrystalline with Zn vacancies	[23]
(2015)	0.55	525	Polycrystalline	[24]

Table 1. List of reported zT of ZnSb.

2. Crystal structure of ZnSb

2.1. Crystallographic structure and covalent bonds

The crystallographic structure of ZnSb has been determined by Almin [8]. According to this determination, ZnSb has orthorhombic crystal structure, oP16 and belongs to the space group Pbca no. 61. The structure of ZnSb has been studied and confirmed by different techniques, albeit gave slightly different interatomic distances [25–28]. **Figure 2** shows the crystal structure of ZnSb that was generated by the structural data from Mozharivskyj [27].

The crystal structure can be viewed as a deformed zinc blende structure. The distorted edge-sharing $ZnSb_4$ tetrahedra generate a peculiar five-fold coordination of each atom, as seen in **Figure 2a**: one of the same kind and four of the other kind. In the context of bonding and its relation to conduction, all atoms in the crystal structure are tied together in a network—a point, we will return to below.

Another way to systematize the structure is to group the atoms together in planar rhomboid rings of Zn_2Sb_2 that have short Zn-Zn bonds connected to two different longer Zn-Sb bonds, as seen in **Figure 2a**. These motifs are also tied together in a network that completes the crystal structure. The crystal structure can be recognized in atomic scale by scanning transmission electron microscopy (STEM), as shown in **Figure 2b**.

The interatomic distances for each bond are also annotated in **Figure 2a**. The bonds in ZnSb have been categorized in three groups, shown in **Figure 2c** and **d**: the bonds $i-vi$ are covalent

bonds for building up the tetrahedron; the bonds *vii* and *viii* form the Zn_2Sb_2 -ring; and the bonds ix_{1-6} are the dimers that connect the Zn_2Sb_2 -rings. The angles between each Sb-Zn-Sb bond are also annotated in **Figure 2d**. Notice that the angles are close to those in regular tetrahedron, 109.5° . Therefore, even though the structure has five-fold coordination, one can still expect that ZnSb satisfies the tetrahedron rules to some extent. One of them is the electron count per bond. ZnSb has seven valence electrons per formula unit, whereas a regular tetrahedral binary semiconductor has eight valence electrons. Such electron-poor valence often indicates a metallic bond. Yet, ZnSb behaves as a semiconductor. The clue about its semiconducting property is probably due to the sp^3 -hybrid orbitals in the tetrahedron, that often represents a semiconducting bond [30]. The counting rules cannot be applied on a per-bond-basis without considering the complete network. Therefore, all the atoms in the crystal structure are bonded together in a network. ZnSb, thereby, has been classified as an electron-poor framework semiconductor (EPFS) [26, 31]. A quite similar interpretation for the structure has been applied to the related compounds CdSb [30, 32–34] and ZnAs [35].

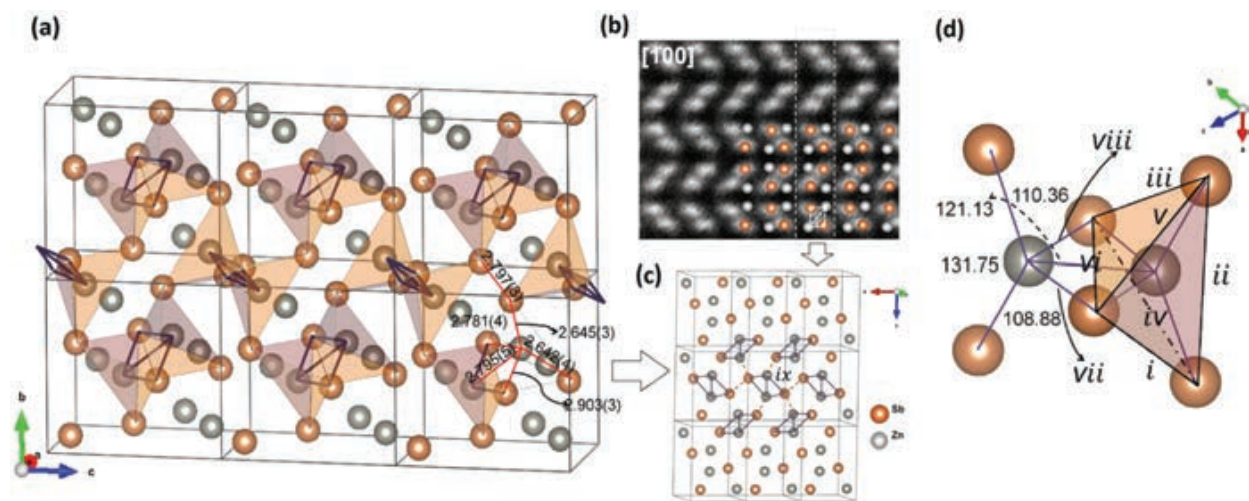


Figure 2. Crystal structure, bonding and coordination environment of ZnSb. (Reprinted with author's permission from [29]. ©X. Song, 2016.) (a) Structure in a $1 \times 2 \times 3$ cell generated by Mozharivskyj's data [27]. Both the deformed tetrahedra and the Zn_2Sb_2 -ring, as well as the interatomic distances between the nearest neighbours are annotated. (b) High-resolution scanning transmission electron microscopic (HR-STEM) imaging reveals atomic scale structure that is recognized corresponding to (a) and (c). (c) $3 \times 1 \times 3$ cell shows the Zn_2Sb_2 -ring network. Each ring has six nearest neighbours, connected by bonds ix_{1-6} . (d) The angles between Sb-Zn-Sb are similar to that of the standard tetrahedron, 109.5° . The bonds *i-vi* are covalent bonds for building up the tetrahedron, while *vii* and *viii* are the bonds to form Zn_2Sb_2 -ring; bonds ix_{1-6} in (c) are the dimers, that connect the Zn_2Sb_2 -rings.

Valence electrons in ZnSb have a certain distribution. **Figure 3** shows the theoretical *ab-initio* calculations by GGA-PBE (Generalized Gradient Approximation with Perdew-Burke-Ernzerhof exchange functionals) of the so-called deformation charge [36].

The results show that a Zn atom transfers a small average fraction of 0.26 electrons to Sb along Zn-Sb bond [37], which is expected due to the difference in Pauling electronegativity between Zn (1.65eV) and Sb (1.96eV). Essentially, the same transfer was found in the calculations of Benson *et al.* [38]. On the other hand, X-ray photoelectron spectroscopy (XPS) and electron energy loss spectroscopy (EELS) measurements indicated a shift of a Zn Auger peak and softening of EELS fine structure could be caused by a small net charge transfer of 0.1 electron

from Zn to Sb [39]. The apparent difference between reported experiments and calculations can be related to experimental uncertainties and different volumes that were chosen for the calculation.

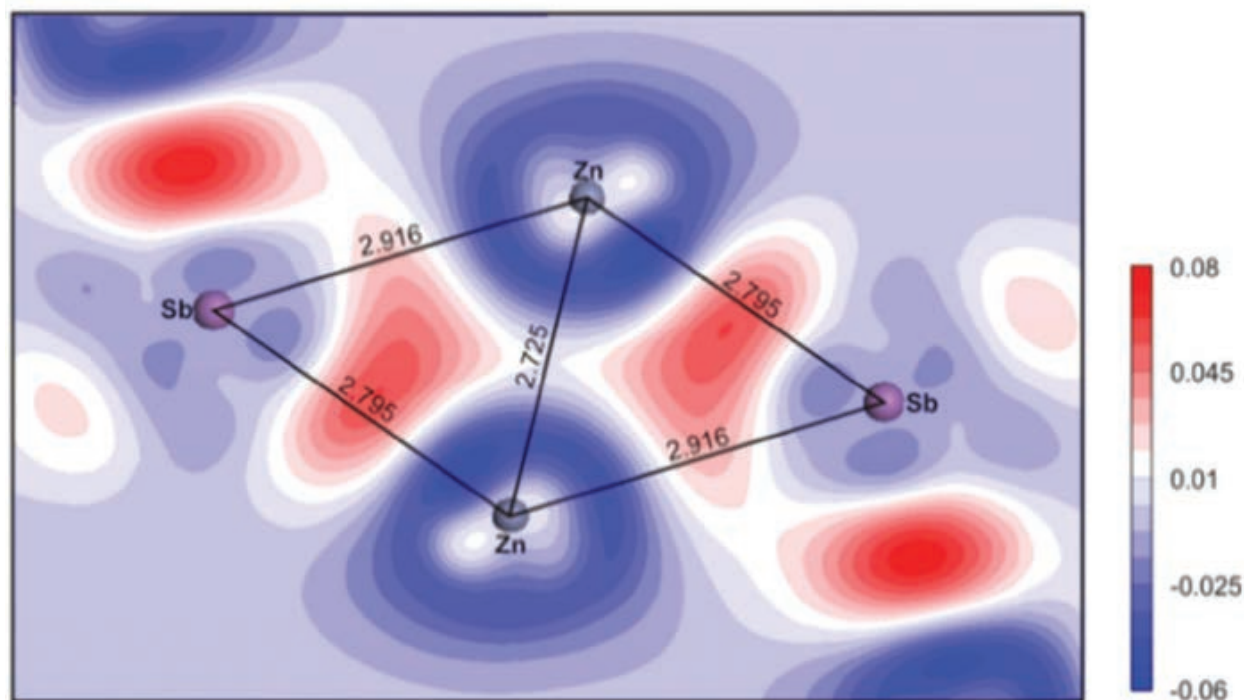


Figure 3. Deformation charge density distribution in electron per Å² in the plane of a Zn₂Sb₂-ring calculated by GGA-PBE. The colour map indicates the isocharge density lines: red indicates accumulation of electrons, whereas blue shows loss of electrons in the relaxed structure of the compound compared with the number of electrons in the free atoms [36]. (DOI:10.1088/0953-8984/26/36/365401. © IOP Publishing. Reproduced with permission. All rights reserved.)

2.2. Electronic structure

2.2.1. Band calculations

The band structure of ZnSb has been calculated by *ab-initio* methods by many groups in recent years [2, 26, 31, 36–42]. The calculations are based upon density functional theory (DFT), but with varying detailed approximations and trade-offs between computational cost and accuracy. By comparing different calculated band diagrams, one can see some features that are common for most of the calculations and expect to filter out methodological errors in the different reports. **Figure 4** shows calculation of ZnSb band diagram.

The zero energy position corresponds to the largest energy of filled states. Thus, the states below 0 correspond to the valence band, while those above correspond to the conduction band. The value of the band gap is severely underestimated by the computational approximations. By using more accurate methods but at the expense of increased computation time, such as HSE-hybrid functional (Heyd-Scuseria-Ernzerhof), the band gap was calculated to be around 0.5eV [37]. This value is close to the experimental value for single crystal ZnSb. On the other hand, the shape of the bands may be less affected by computational approximations. The band diagram in **Figure 4** shares some of the features found in most of the calculations listed. The band gap is indirect with the maximum of the valence band along the symmetry

line Γ -X and the minimum of the conduction band along Γ -Z. One can see that the conduction band contains more satellites within 0.5eV of the minimum than pockets of the maximum in the valence band. Thus, one can expect ZnSb would have acted better as an n -type material than a p -type material, if stable n -type doping could have been achieved.

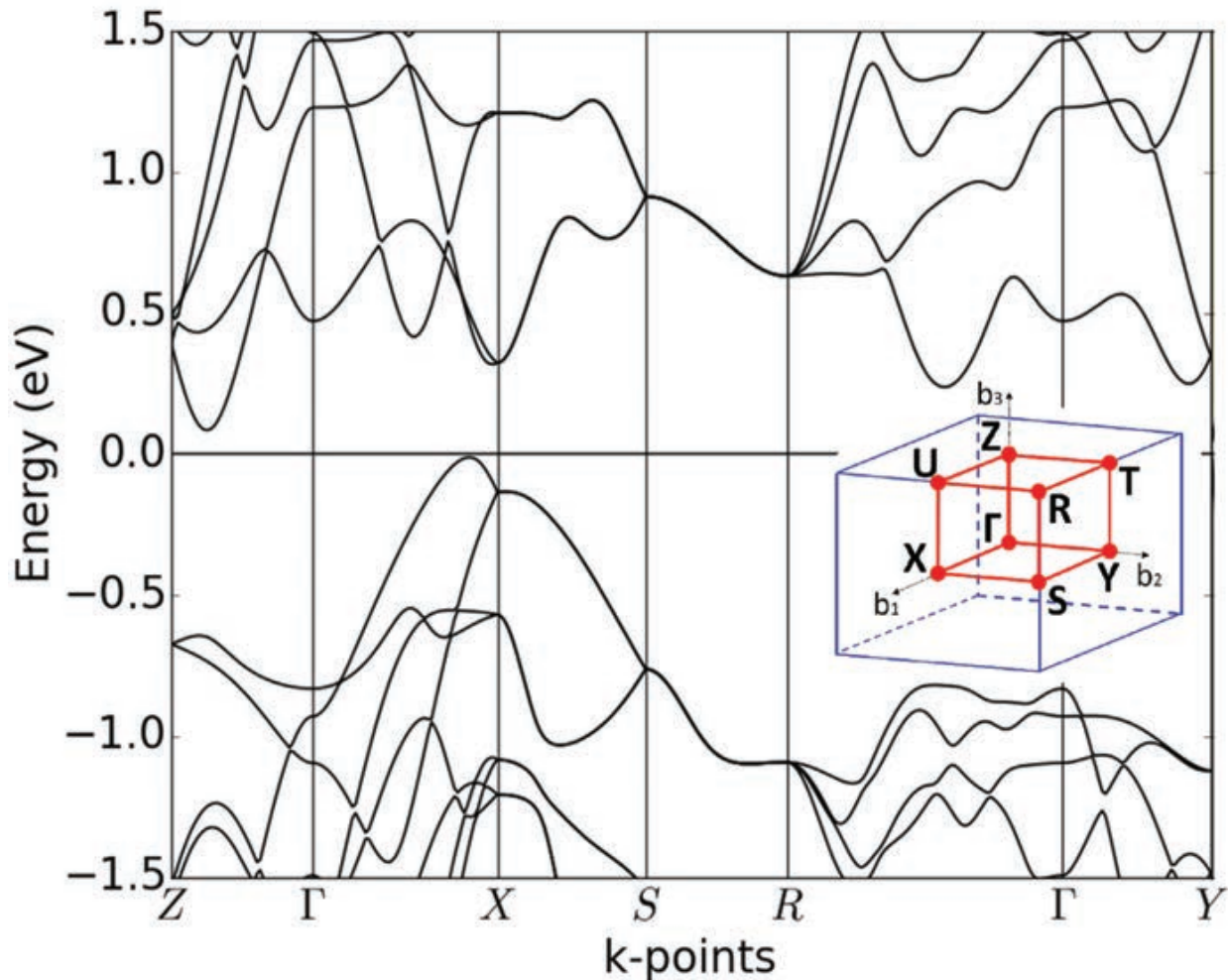


Figure 4. Band diagram of ZnSb showing energy states along high symmetry directions in k -space calculated by Berland *et al.* [2] using GGA–PBE. The Brillouin zone for orthorhombic lattice with the high symmetry symbols are shown in inset for indication. (Reprinted with author's permission from [29]. ©X. Song, 2016.)

It is worth mentioning the band diagram that was calculated by Yamada in 1978 by using pseudopotentials [43]. The maximum of the valence band was found to be on the line from Γ -X at $k=(0.93\pi/a, 0.0)$, which is close to the DFT values, and the band gap was 0.6eV. However, a minimum of the conduction band is located at $k=(0.47\pi/a, 0.0)$ along Γ -X, which is not in agreement with most DFT calculations, and it is hard to determine experimentally due to the difficulty in preparing n -type ZnSb.

2.2.2. Experimental band gap

The band gap has been measured by different methods. Values of 0.5–0.53eV for single crystal ZnSb, which were measured by optical absorption, have been reported [44, 45]. These values

are essentially identical when considering the uncertainties, and 0.5 eV has been considered to be a reference value for single crystal ZnSb. Many research have also determined the thermodynamic band gap from the temperature dependence of the charge carrier concentration in the intrinsic regime. The charge carrier concentration is determined from the Hall coefficient, R_H . A linear fit of $\ln R_H T^{\frac{3}{2}}$ vs. $\frac{1}{T}$ will yield the activation energy, which is half of the thermodynamic energy gap. (This assumes an effective density of states proportional to $T^{\frac{3}{2}}$). Values of 0.47–0.65 eV have been reported in the literature for single crystal ZnSb based upon Hall effect measurements [46, 47].

For polycrystalline ZnSb, the band gap is often reported to be around 0.31–0.35 eV [13, 48], which is smaller than that of single crystal material. It is justified to discuss whether the band gap really is different, or if it is due to that the idealizations of the measurement methods do not hold for polycrystalline material. One of the methods that has been used for estimating the band gap is to measure the temperature dependence of the Seebeck coefficient. By determining the temperature, T_{max} , for the maximum of the absolute value of the Seebeck coefficient, α_{max} , the band gap can be estimated from the Goldsmid formula, $E_g = 2q\alpha_{max}T_{max}$ [49]. This method works well for many semiconductors, for instance Zr-NiSn half-Heusler [50]. However, there have been reports on some systems that the Goldsmid formula does not apply [51, 52]. ZnSb may be one of them. Guo and Luo have reported that the Goldsmid formula returned a value of $E_g=0.3$ eV for their polycrystalline ZnSb samples [23]. However, Böttger *et al.* justified that for the samples that have a band gap of 0.3 eV obtained by Goldsmid formula, the temperature-dependent resistivity was fitted better with a value of 0.44 eV [53]. It is fair to state that it depends upon the context whether it is best to reconsider the band gap value for polycrystalline or reconsider the idealizations used in the measurement methods.

We should also keep in mind that heavily doping may influence the density of states near the band edges, forming tails that are extending into the band gap. The defect states in the band gap also influence the E_g values. This is a well-documented phenomenon (for Si) [54], even if the precision in a detailed quantitative understanding may be lacking. We have reported that the maximum of the Seebeck coefficient of ZnSb could be varied considerably by the presence of defect states in the band gap [52].

2.2.3. Effective mass and density of states

The idealized single parabolic band (SPB) model is convenient for analysing experimental results. The model has been successful for finding the optimum doping concentration of many thermoelectric materials [55–57]. When applied to Seebeck measurements on ZnSb with different doping concentrations, it has been observed that Pisarenko plot (the Seebeck coefficient vs. the charge carrier concentration) does not follow the SPB model with a single density of states effective mass m^* , which was determined to be $(0.42–0.49) \times m_0$, where m_0 is free electron mass [15, 53], but rather a different mass fit for different ranges of doping concentrations. A previous study by Böttger *et al.* has suggested that deviations from idealized SPB behaviour could be induced by impurity band states [53]. We have showed that deviations from simple SPB behaviour at varying doping concentration could be modelled by introducing an impurity band [52]. One may comment that the best fit with varying m^* is not necessary to imply that

the energy band curvature varies. It suffices that the temperature-dependent position of the Fermi level varies differently than that in an idealized SPB case.

3. Electrical properties and doping effect

3.1. Electrical properties and scattering mechanisms

Table 2 summarizes the band gap, the charge carrier concentration and other electrical and thermal properties reported for ZnSb in the literature.

Given the crystal structure, single crystal ZnSb exhibits anisotropic conduction, which is strongly dependent on the anisotropic effective mass [58]. Böttger *et al.* determined each mass tensor component from band diagram calculations [53]. Different components were given by $m_a^* = 0.1811m_0$; $m_b^* = 0.4913m_0$; $m_c^* = 0.0837m_0$. The results agree with the anisotropic Hall mobility and the highest electrical conductivity is measured along the *c*-axis [15, 45]. Anisotropic energy surface has also been observed by optical absorption indicating that the constant energy surface in *k*-space in ZnSb is a spheroid [59].

There is much literature devoted to scattering mechanisms in semiconductors [65], while there are fewer reports dealing with that topic specifically for ZnSb. It is expected that ZnSb has similar behaviour to those semiconductors which have been much studied and follows similar trends. ZnSb appears to have favourably small polarity due to small electronegativity difference between Zn and Sb. This would in turn lead to a negligible polar optical phonon scattering compared to III–V and II–VI compounds where polar optical phonon scattering may be dominant. Roughly, transport in ZnSb is dominated by impurity scattering at low temperature, while at higher temperature, when lattice vibrations are stronger, longitudinal acoustic phonon scattering dominates (deformation potential scattering). The hole mobility varies with temperature as $\mu \propto T^r$, thus a plot of $\ln\mu$ vs. *T* will give the scattering factor *r* that implies the scattering mechanism. A value of -1 to -1.5 typically indicates that longitudinal acoustic phonon scattering dominates. In **Figure 5a**, the slopes of the Hall mobility approaches -1.5 as the doping concentration decreases. It indicates that acoustic phonon scattering dominates within the temperature range. The deviation from -1.5 for each individual curve is attributed to additional ionized impurity scattering [66]. It is also seen that the higher hole concentration corresponds to an increase in ionized impurity scattering, which limits the hole mobility.

Not only the intentional dopants, but also defects, that are ionized or neutralized, screened or unscreened, contribute to scattering. Likely scattering centres are Zn vacancies, interstitials, internal strain, grain boundaries and dislocations. **Figure 5b** shows the resistivity for an unprocessed ZnSb ingot that was obtained directly from solidification and hot-pressed ZnSb pellets with different dopant concentrations. The temperature coefficient, $\frac{d\rho}{dT}$, for the unprocessed ingot is positive, which is commonly observed for metals and semiconductors in a certain temperature range where phonon scattering dominates. For the processed samples, either with or without Ag, the temperature coefficient $\frac{d\rho}{dT}$ is negative. The reason for the negative temperature coefficient could be the dominant Coulomb scattering due to charged defects or impurities.

Reference	Report year	Structure	Dopant	σ (S)	ρ ($\Omega\cdot\text{cm}$)	μ ($\text{cm}^2/(\text{V}\cdot\text{s})$)	p (cm^{-3})	α ($\mu\text{V}/\text{K}$)	E_g (eV)	κ (W/(m·K))
[60]	(1947)	–	–	–	0.0072	–	–	250	–	1.4
[9]	(1954)	–	2at.% Sn+0.1at.% Ag	–	0.0019	–	–	210	–	–
[61]	(1960)	Single crystal	–	2.8	3.57	350	5.1×10^{16}	440	0.52–0.57	–
[46]	(1961)	Single crystal	–	3	0.33	480	3×10^{16}	550	0.49	–
[62]	(1963)	Single crystal	–	1.6	0.63	248	4.1×10^{16}	–	–	–
[62]	(1963)	Single crystal	–	5.6	0.18	1150	3.1×10^{16}	–	–	–
[45]	(1964)	Single crystal	–	6.4	0.16	10	4×10^{18}	110	0.53	1.1
[14]	(1964)	Single crystal	–	19.7	0.05	384	3.2×10^{17}	490	–	–
[14]	(1964)	Polycrystalline	–	20	0.05	95.2	1.3×10^{18}	375	–	1.3
[14]	(1964)	Polycrystalline	0.1at.% Ga	2.04	0.49	210	6×10^{16}	675	–	–
[14]	(1964)	Polycrystalline	0.1at.% Cu	110	–	680	1.1×10^{18}	–	–	–
[63]	(1964)	Single crystal	–	–	–	–	3×10^{17}	–	0.48	–
[15]	(1966)	Single crystal	–	825	0.001	800	2×10^{16}	182	–	3.7
[15]	(1966)	Single crystal	Cu	42	0.02	660	4×10^{17}	–	–	–
[15]	(1966)	Single crystal	Cu	898	0.001	510	1×10^{19}	–	–	–
[47]	(1967)	Single crystal	Au	26.9	0.04	233	4.2×10^{17}	404	0.47–0.65	–
[47]	(1967)	Single crystal	In	37.5	0.03	326	7.7×10^{17}	288	0.47–0.65	–
[47]	(1967)	Single crystal	Te	51	0.02	379	8.3×10^{17}	400	0.47–0.65	–
[16]	(2010)	Polycrystalline	2wt.% Ag	–	0.01	–	–	185	–	2.3
[17]	(2010)	Polycrystalline	–	28.2–32.1	–	–	–	400–500	–	1.41
[19]	(2013)	Polycrystalline	0.002at.% Ag	–	0.0016	111	2.6×10^{19}	181	–	1.5
[20]	(2014)	Polycrystalline	Sn	180	–	–	4.9×10^{18}	250	–	1.8
[64]	(2014)	Polycrystalline	Cu	640	–	–	2.5×10^{19}	134	–	–
[21]	(2014)	Polycrystalline	0.15at.% Cu	935	–	–	2.4×10^{19}	142	–	–
[23]	(2015)	Polycrystalline	3at.% V _{Zn}	800	0.0012	66	7.9×10^{17}	275	0.29	1.75

Table 2. Summary of electrical properties of ZnSb.

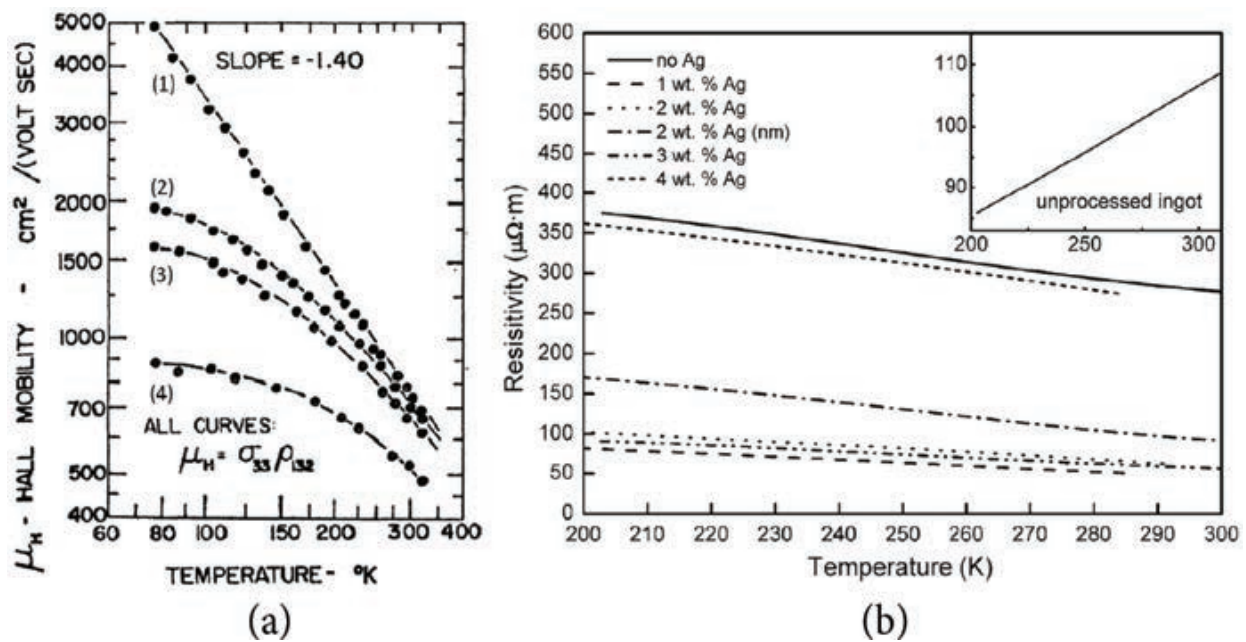


Figure 5. (a) Hall mobility along the *c*-axis as a function of temperature for *p*-type ZnSb at various hole concentrations (1) 3×10^{16} cm⁻³; (2) 4×10^{17} cm⁻³; (3) 5.5×10^{17} cm⁻³; (4) 1×10^{19} cm⁻³. (Reprinted with permission from [15]. Copyright (1966) by the American Physical Society.) (b) Resistivity vs. temperature of ball-milled and hot-pressed samples with varying silver content. Inset: unprocessed sample (Ingot) [16]. (Reprinted with permission of Springer.)

3.2. Doping effects

The most direct purpose of doping is to vary the charge carrier concentration. A broad range of dopant elements has been reported for ZnSb. The selection of dopant is often rationalized based on the same valence electron counting scheme that is applied to the elemental group IV, III-V or II-VI tetrahedrally bonded semiconductors. These considerations are applied for acceptors, while donors are challenging. One will have acceptors by replacing group I elements for Zn or group IV elements for Sb. It is expected that donors can be substitutes for group III elements on Zn sites and group VI elements on Sb sites. In all cases, there may be an issue with doping efficiency, i.e. not all the added dopant atoms will be electrically active. It is common and qualitatively well-understood for other semiconductors that this inefficiency involves segregation (solid solubility limit), clustering of dopant atoms and/or agglomeration of complexes of dopant atoms and point defects. A theoretical calculation predicts that the optimum hole concentration for the thermoelectric efficiency of ZnSb is around 2×10^{19} cm⁻³ [53], which is achievable in *p*-type ZnSb. For donors in ZnSb, there may also be additional issues to what has been mentioned above.

3.2.1. Acceptors

3.2.1.1. I_{Zn} —acceptors as elements of group I

Cu_{Zn} , Au_{Zn} , Ag_{Zn} all yield *p*-type conduction [47, 67]. Most of the reported charge carrier concentrations are below the optimum value, and probably depend upon the details of sample

preparation. However, the highest hole concentration that have been reported for Ag doping is $4 \times 10^{19} \text{ cm}^{-3}$ (for 0.02 at.% Ag) [19] while that for Cu is $2 \times 10^{19} \text{ cm}^{-3}$ (for 0.1 at.% Cu) [15, 21, 64]. There are several interesting behaviours that involve additional states in the band gap when doping with Cu. Some details can be seen in [52].

3.2.1.2. IV_{Sb} —acceptors as the elements of group IV

Hole concentrations around $(4\text{--}14) \times 10^{18} \text{ cm}^{-3}$ were obtained in materials with a content of (0.06–3) at.% Sn [53, 68]. The hole concentration variations with Sn doping concentrations were apparently opposite for these two studies. The highest hole concentration of $14 \times 10^{18} \text{ cm}^{-3}$ was obtained for content 0.1 at.% Sn [68] and yielded the highest mobility. It was suggested that two different doping mechanisms are effective in different temperature ranges involving different intrinsic defects, Sn on different lattice sites and their variation with temperature [68].

3.2.1.3. $I_{Zn}IV_{Sb}$ —co-doping

Hole concentrations of $(2\text{--}2.5) \times 10^{19} \text{ cm}^{-3}$ have been reported by co-doping of group I (0.15 at.% Cu or Ag)/IV (0.6 at.% Pb, Sn, or Ge)/Cd [20, 21]. The measured transport coefficients at different regions indicate two types of impurity acceptor: one embedded into Zn sites, and another into Sb sites. Here, Cd is not expected to act as an acceptor, but for increasing the phonon scattering and thereby reducing the thermal conductivity. A similar intended function has been applied by adding P to increase alloy phonon scattering in the Cu doped ZnSb [18, 69].

3.2.2. Donors

n-Type ZnSb is desired because (i) thermoelectric modules are preferably built of parallel legs of *n*-type and *p*-type materials, and it is preferable to use the same material (ZnSb) for minimizing the thermal stress; (ii) theoretically, *n*-type ZnSb is believed to be a much better thermoelectric material than *p*-type [36, 40, 42]. However, no real successful stable *n*-type doping has been achieved. But, temporary *n*-type behaviours have been reported by doping with group III and group VI elements.

3.2.2.1. III_{Zn} —donors as elements of group III

Group III elements have been used as donors to yield *n*-type conduction in CdSb [70]. It was later reported that ZnSb could also be made *n*-type by In doping, probably substituting Zn as In_{Zn} . Al_{Zn} and Ga_{Zn} also exhibited temporary *n*-type behaviour [71, 72]. However, the *n*-type conduction did not always occur. Justi *et al.* did not achieve *n*-type ZnSb with Ga despite several attempts with single and polycrystalline ZnSb [14]. Niedziolka *et al.* predicted theoretically by DFT calculations that boron would electronically be a good candidate for *n*-type ZnSb, but did not succeed to synthesize the material and ascribed it to the high formation energy of a boron atom on a Zn site [36].

3.2.2.2. VI_{Sb} —donors as elements of group VI

Some success with Te doping has been reported. Ueda *et al.* reported that a Te content in very narrow window around 2at.% yielded *n*-type, possibly by forming substitutions of Te atoms on Sb sites, Te_{Sb} ; while at lower concentration (<1at.%) and higher concentrations (>3at.%), the samples are always *p*-type. Excess doping with Te results in precipitation of the ZnTe phase and a change in conduction from *n*- to *p*-type [73]. No *n*-type doping was observed by S doping [29].

3.2.2.3. *n*-Type to *p*-type transition

A temporary *n*-type behaviour with a transition to *p*-type has been reported. Explanations for these behaviours are related to such factors as oxygen migration on internal surfaces or grain boundaries [71]. Schneider has reported an *n*-type to *p*-type transition in *n*-type $Zn_xCd_{1-x}Sb$ every time when an oxygen gas was flushed into the sample container, and relaxed back to *n*-type after a certain time [71]. Another factor entering into explanations are Zn vacancies acting as acceptors and their migration [36, 42, 74]. A similar transition from *n*-type to *p*-type also occurs in the related compound CdSb, which has been attributed to Cd-vacancies [75].

4. Zn vacancies and intrinsic defects

The theoretical intrinsic charge carrier concentration of perfect ZnSb at room temperature is approximately $2 \times 10^{14} \text{ cm}^{-3}$ given by $p_i = 2 \left(\frac{2\pi m^* k_B T}{h^2} \right)^{\frac{3}{2}} e^{\eta}$, where $\eta = -\frac{E_g}{2k_B T}$, and taking $E_g = 0.53$ eV and $m^* = 0.42 \times m_0$ [15]. However, the experimental measurements show that the charge carrier concentration of the best single crystals at room temperature is around $(1-2) \times 10^{16} \text{ cm}^{-3}$ [15, 46, 61, 62] and up to $\sim 10^{18} \text{ cm}^{-3}$ for polycrystalline samples without intended dopants [14, 45]. This deviation is considered due to the intrinsic defects, giving a net hole concentration. The most favoured intrinsic defects in ZnSb are Zn vacancies, which are believed to yield *p*-type conduction [42, 74]. The intrinsic defects in ZnSb have been calculated on by DFT methods [42, 74]. The calculations gave much lower formation energies for Zn vacancies than other intrinsic defects, meaning that Zn vacancies will out-number other intrinsic defects by orders of magnitude. Discrete vacancy defect states are considered to accept electrons from (or donate electrons to) the bands, if they are negatively (or positively) charged. The charge state of the defect will depend on the Fermi level for electrons. This can, in principle, be calculated from the condition of electrical charge conservation (charge neutrality). **Figure 6** shows a conceptual schematic model of a Zn vacancy in different charge states. It is based upon a combination of interpretation of Bjerg *et al.*'s work [74] and a popularization of Fairs Vacancy model for silicon [76].

The vacancy can in principle have any charge states, but only -2, -1 and 0 seem readily accessible by doping and temperature variation. The formation energy for V_{Zn}^- in this configuration was calculated to be 0.32eV. The net hole concentration in ZnSb without any doping was then calculated from the requirement of charge neutrality and assuming equilibrium

number of vacancies in different charge states (-1 and -2 dominated). The net hole concentration in this configuration was calculated to be $8.8 \times 10^{17} \text{ cm}^{-3}$ at room temperature, which is in the range of the experimental Hall concentrations measured by Böttger *et al.* $(4-10) \times 10^{17} \text{ cm}^{-3}$ [16]. One should also compare the calculated net hole concentration to the hole concentration of undoped single crystal ZnSb that is significantly lower than $8.8 \times 10^{17} \text{ cm}^{-3}$. This apparent discrepancy indicates that exact values of formation energies should be used with caution. However, the concepts and the idea of V_{Zn} as a very important defect seem valid.

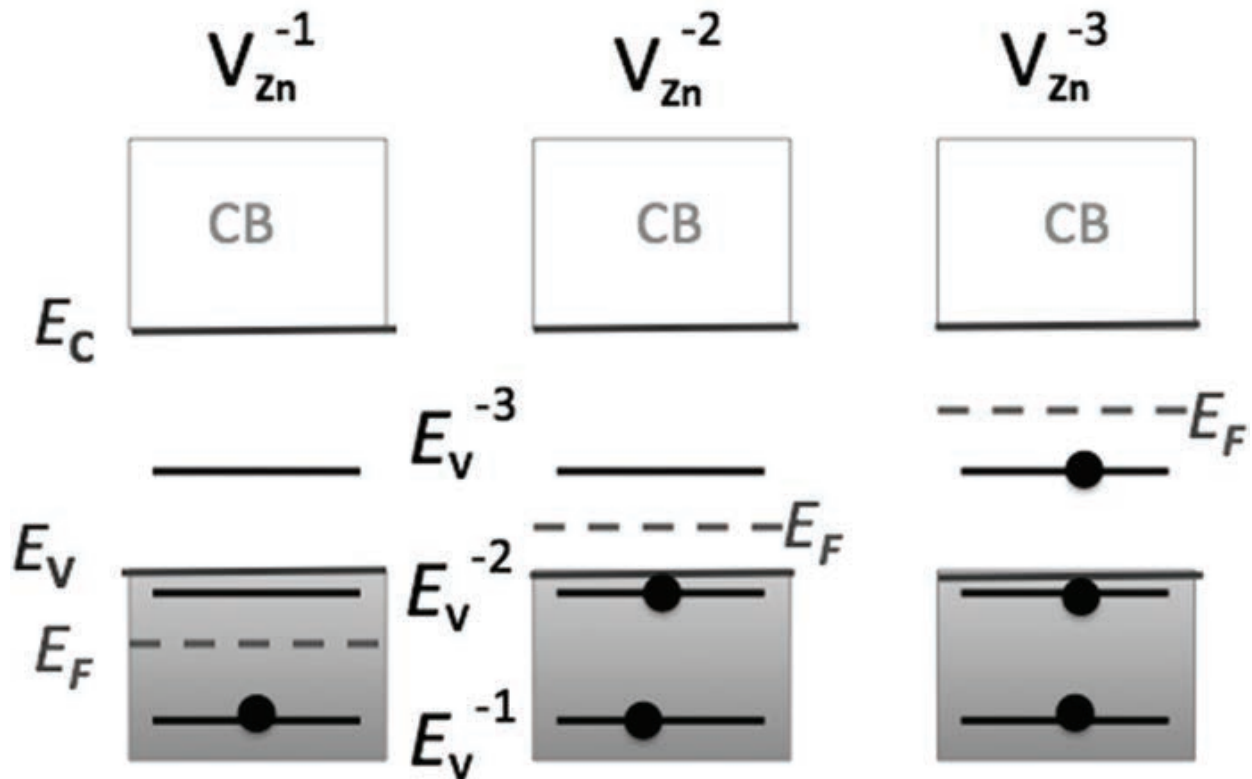
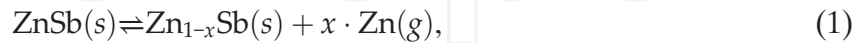


Figure 6. Schematic drawing of occupancy of localized states associated with the Zn vacancy in ZnSb. (Reprinted with author's permission from [29]. ©X. Song, 2016.) The vacancy will have different charge states -1, -2, -3 dependent upon the position of the Fermi level E_F with respect to the levels E_V^{-1} , E_V^{-2} and E_V^{-3} . E_V is the valence band onset and E_C is the conduction band (CB) onset.

There have been many reports on changes in charge carrier concentration after heat treatments, both for single crystal and polycrystalline ZnSb. Many observed a slow recovery to the initial values of the charge carrier concentration [15, 20, 44, 45, 47, 61, 77]. Andronik *et al.* specifically attributed this change to Frenkel defects [77]: by Zn atoms leaving their lattice sites and becoming vacancy-interstitial pairs, $V_{\text{Zn}}\text{-Zn}_i$. By assuming that all of the measured changes in charge carrier concentration were due to Frenkel defect formation, the activation energy of the process could be determined. The Frenkel defect concentration n_φ was assumed to be given by $n_\varphi = \sqrt{NN'} e^{-\frac{E_\varphi}{2k_B T}}$, where $n_\varphi = n_i - n_0$ is the concentration of Frenkel defect, n_0 and n_i are the concentration before and after heating, respectively, N is the concentration of atoms, N' is the concentration of interstitials (there are more than one interstitial position in the lattice), E_φ is the formation energy of a Frenkel pair. The formation energy was determined

from experiments to be 0.5eV. This experimental value seems in the range of formation energies calculated by Bjerg *et al.* [74]. On the other hand, the formation energy for a Zn vacancy calculated by Jund *et al.* gave a different value of 0.8eV [42]. This calculation used a $\text{Zn}_{64}\text{Sb}_{64}$ supercell with 128 lattice sites and compared it to the energy of a $\text{Zn}_{63}\text{Sb}_{64}$ supercell at 0K, which corresponds to a vacancy concentration of 1.5at.%.

Recently, we have studied evaporation of Zn by thermogravimetry and Zn vacancy created during vaporization [29]. The net hole concentration was measured to be about $6 \times 10^{18} \text{cm}^{-3}$, corresponding to a vacancy concentration of about 0.03at.%. Schematically, two processes in series were considered as:



Reaction (1) occurs when the V_{Zn} was created but within the dilute limit, while reaction (2) applies to a situation where the Zn vacancy concentration is beyond the solubility limit and ZnSb decomposes into Sb phase and Zn vapour.

5. Impurity band conduction

In an idealized semiconductor, which is well-approximated by pure Si crystals [78], the charge carrier concentration shows the so-called freeze out at low (cryogenic) temperatures: the dopant atoms are not ionized and the charge carrier concentration goes towards zero, characterized by an infinite Hall coefficient in Hall measurements. However, the Hall coefficient in undoped ZnSb has shown a turning point at low temperatures, typically below 50K, as seen in **Figure 7**, and then a decrease with further cooling, which is explained by impurity band conduction [79]. Here, the term impurity band is most likely tied to defects, but observed phenomena are similar to what can be observed for high doping concentration in semiconductors. Impurity band conduction has been reported in many materials [80–82]. It was also observed for ZnSb by Justi *et al.* in the 1960s [14]. Recently, several others have reported on impurity bands in ZnSb [53, 79, 83].

Let us here analyse sketchily the conditions for observing the characteristics shown in **Figure 7**. The specifics of this observation are given in [79]. The changes in hole concentration as the sample was cooled is in principle similar to that of a textbook low doping concentration semiconductor, where the charge carriers are frozen out of the valence band. The valence band of the sample in **Figure 7** will be nearly empty (for holes) at the lowest temperature. The holes are transferred to the acceptor-based impurity band. However, the holes are mobile in the impurity band and contribute to conduction and Hall effect. Thus, the Hall coefficient decreases with cooling to the lowest temperatures. In order to get conduction in the impurity band, some donor compensating centres are needed. (Without donor level, the impurity band would be full of holes, i.e. empty for electrons and there is no conduction).

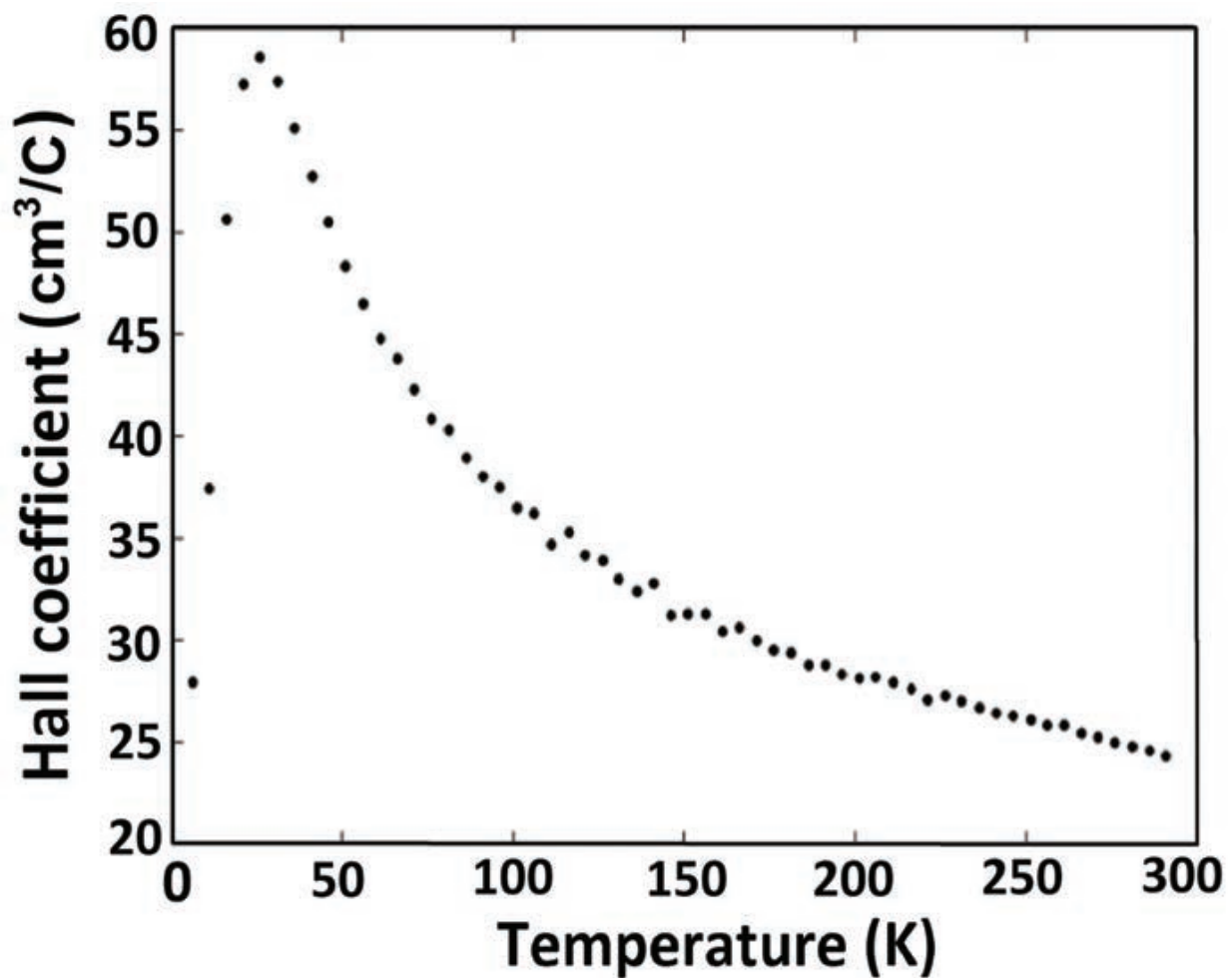


Figure 7. The Hall coefficient of an undoped hot-pressed ZnSb sample. (Reprinted with author's permission from [29]. ©X. Song, 2016.) The Hall coefficient in ideal cases is inversely proportional to the charge carrier concentration. If there was regular freeze-out of the charge carriers, the Hall coefficient goes to infinity at low temperatures. However, in the presented case of undoped ZnSb, there is a turning point in the Hall coefficient, which was interpreted as a signature of an impurity band.

We turn to a situation where the doping concentration is much higher than that of the sample in **Figure 7**, and first consider the large difference in characteristic features of the change in the charge carrier concentration with temperature. **Figure 8** compares the Hall concentration of the charge carrier and the Hall mobility (inset) at low temperature for high (0.3 at.% Cu) and lower concentration (no Cu), respectively (data in Refs. [52, 79]). One can see that the characteristic feature of impurity band conduction vanished in the highly doped sample at low temperature. The situation is qualitatively as follows: A highly doped sample is equivalent to a degenerate semiconductor, where the hole concentration is high and the Fermi level is located in the valence band. The native impurity band would be full of holes and so would the top of the valence band. At the lowest temperatures, the conduction will occur within the valence band. Therefore, one cannot have a similar change with temperature as in the case of undoped ZnSb where there was a vanishing conduction in the valence band at the lowest temperature.

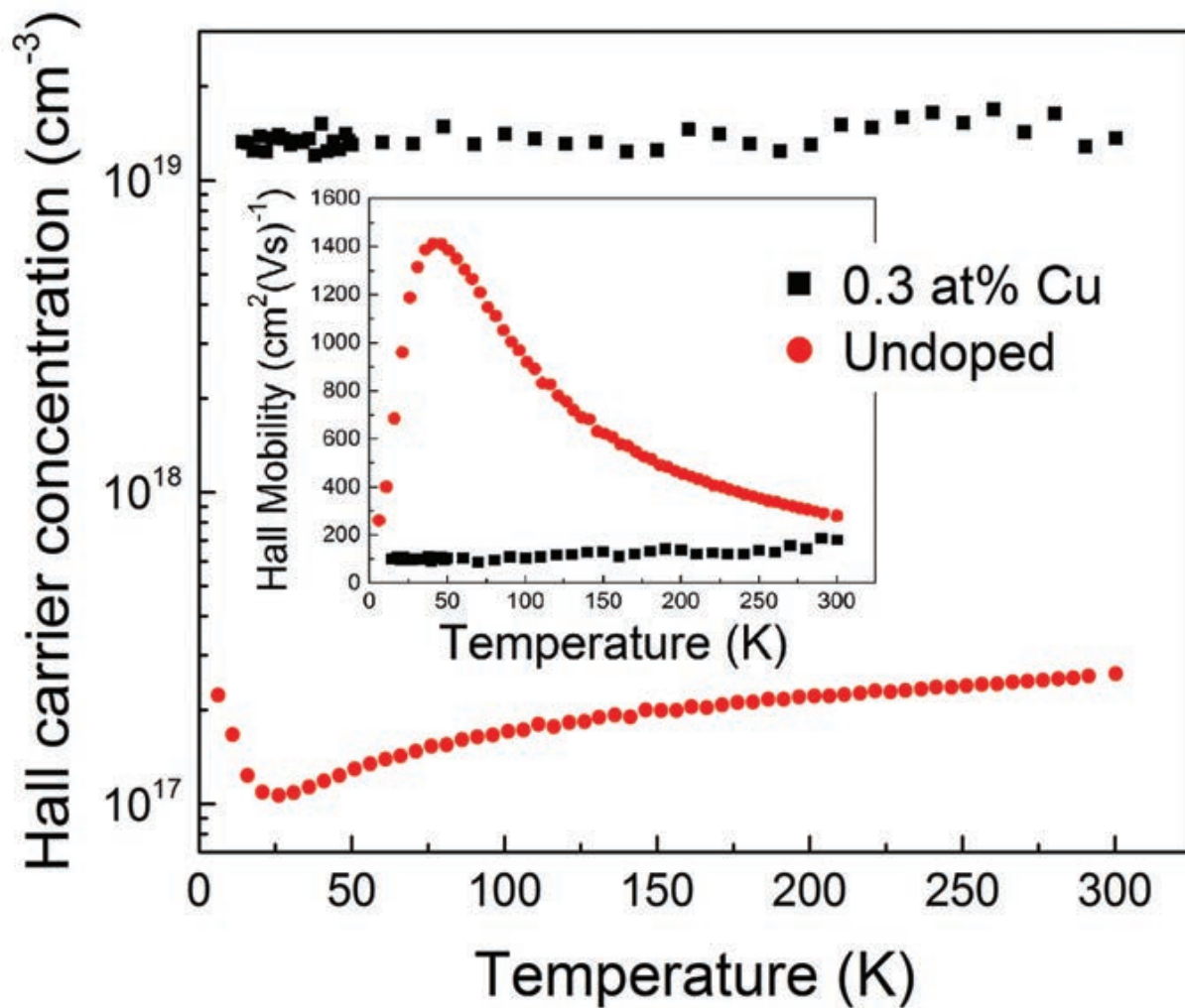


Figure 8. Temperature dependence of the Hall concentration of charge carriers at the temperature lower than 300K of highly doped ZnSb (0.3at.% Cu content) and undoped ZnSb. (Reprinted with author's permission from [29]. ©X. Song, 2016.). Inset: the Hall mobility.

5.1. The impurity band in ZnSb—its nature, origin and specific points of interest

The nature and theoretical treatment of general impurity band can be found in textbooks [84]. The band states are considered to come from interactions, which set in for concentrations above a certain value of defect species, such as dopant atoms, impurities or intrinsic crystal defects.

The formation of impurity band is illustrated in **Figure 9** for an *n*-type semiconductor. Electrons at a donor level can be transferred to a neighbour donor by thermal activation and tunnelling, but without entering into states in the conduction band. One would then have the hopping regime for transport in the material as illustrated in **Figure 9a**. When the donor concentration increases further, the wave functions of the donor states overlap and can form a band, where one has impurity band conduction, as illustrated in **Figure 9b**.

The mobility in the impurity band is typically small because the band is relatively narrow, and as a consequence, one would have a small dispersion curvature in $E(\vec{k})$ and large effective

mass. In a semiconductor, at low temperature, conduction can occur dominantly in the impurity band if there are some compensating levels, such that the impurity band is not fully occupied. At a particular higher concentration, there may be a smear of the impurity band and the conduction band, as illustrated in **Figure 9c**. Beyond this concentration, the Mott transition, which is a sharp transition from insulator to metal behaviour, can take place.

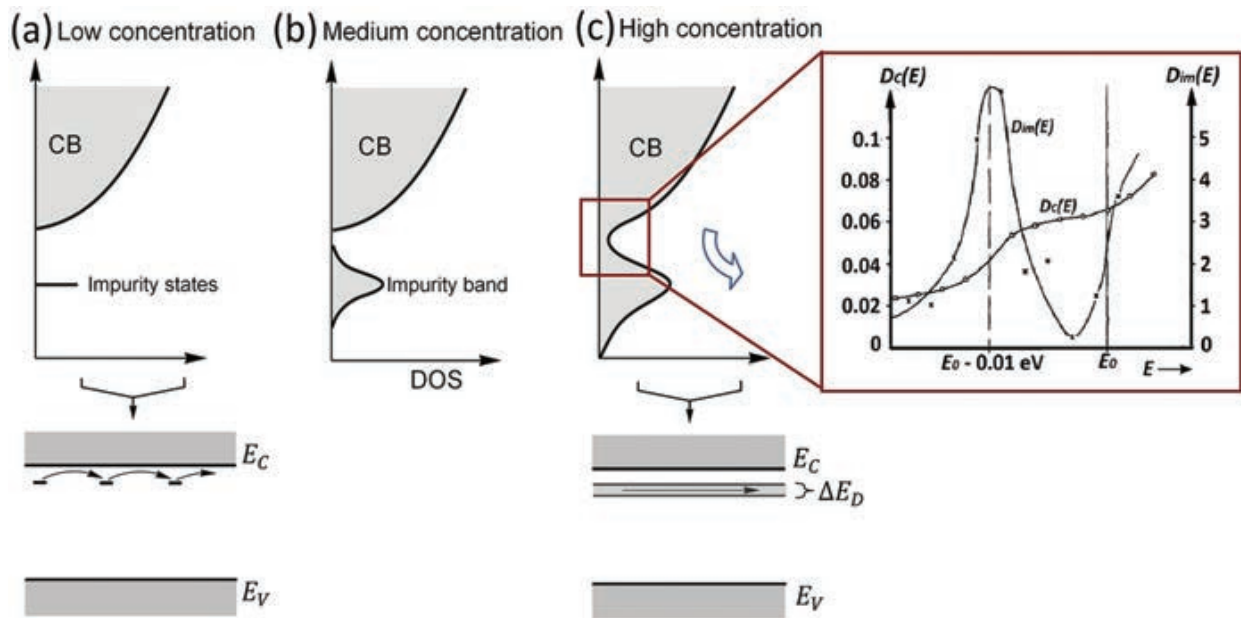


Figure 9. Schematics of impurity state/band and conduction band (CB) for *n*-type semiconductor at low impurity concentration, medium concentration and high concentration at random impurity distribution. Band diagrams illustrate the hopping conduction and impurity band conduction. (Reprint with author's permission from [84]. ©E. Fred Schubert, 2015). Inset: dimensional schematic calculated density of states for high impurity concentration. E_0 is assumed to be the onset of the conduction band; $D_c(E)$ is the number of conduction band and $D_{im}(E)$ is the density of states of impurities in periodically arrangement. (Reprinted with permission from [85]. Copyright (1953) American Chemical Society.)

Usually, the Mott criterion for when the transition occurs is $N_I \geq 0.014 a_B^{-3}$, where N_I is the atomic concentration of impurities and a_B is the Bohr radius of the impurity. There are several different treatments yielding essentially the same numbers [84]. The most considered situations are those of high concentrations of shallow donors or acceptors. Here, the Mott criterion gives the insulator-metal transition. However, one can create impurity bands with a certain energy anywhere in the band gap. Some of the concentrations for the Mott transition then approximately correspond to the concentration to have an impurity band. Rawat *et al.* have suggested a Yb mid-gap impurity band in PbTe affecting the thermoelectric properties [86].

With the doping concentrations for optimum thermoelectric performance that typically is $\sim 10^{19} \text{ cm}^{-3}$, it is reasonable to expect that the formation of impurity bands is rather common in thermoelectric materials. Also, impurity band formation is just one of several high doping effects one should expect, such as the Mott transition, band tailing and band gap renormalization [84]. Thus, one should discuss thermoelectric material in the framework of the theory related to heavily doped semiconductors.

When it comes to ZnSb specifically, it has been estimated that the impurity band may exist for the impurity concentrations that are well within the observed doping concentrations. We have

determined the critical impurity concentration in ZnSb to be about $6 \times 10^{17} \text{ cm}^{-3}$ in previous study, which is around the acceptor concentrations used in the model to fit the low temperature measurements [79]. For the doping concentration of $10^{18} - 10^{19} \text{ cm}^{-3}$ in ZnSb, one can expect impurity bands to form. For undoped or very lightly doped material, we suggested that point defects, especially Zn vacancies can be expected to be involved in impurity bands. From the discussion of vacancy formation in Section 4, it appears likely that a high concentration of vacancies can be created by annealing, even to some extent they could combine with any other possible impurities or defects in impurity band. The impurities will likely be dependent on the specific dopants and the preparation technique. For example, oxygen is expected to be an impurity in ball-milled material and the amount introduced will depend upon the atmosphere during processing. Presently, one cannot make a conclusion about the importance of oxygen in this context and the solid solubility of oxygen is unknown. Fedorov *et al.* observed evidence for impurity levels in the band gap associated with different combinations of group I (Ag or Cu) and group IV (Sn or Ge) acceptor elements, which all were similar to each other, but different to those of the single acceptor element [21]. Temperature-dependent transport coefficients were also measured that were interpreted as a temperature-dependent energy state being present with a level in the valence band. The energy states were considered as hybridized states formed by mixing characteristics of the valence band and the impurity band. In a general case, a temperature-dependent level can have a similar effect as a defect chemistry reaction involving growth and decrease with temperature of the population of two defect species having different energy, as suggested in Ref. [52].

5.2. Impact of impurity band on thermoelectric properties

An impurity band will have an effect on the transport properties and the thermoelectric device properties. It may not be immediately transparent how. The conduction in the impurity band is perhaps a minor effect in this context. The most important effect may be on the Seebeck coefficient.

5.2.1. Effect on conduction

The effect of impurity bands on the electrical conductivity is expected to be largest when holes in the valence band (for *p*-type) do not contribute to the conduction [53]. This is expected to have a strong effect for samples where the doping is below degenerate, but sufficiently close to the Mott criterion, and in addition at low temperatures. It is expected, that in a thermoelectric material, the mobility of the charge carriers in an impurity band is much lower than that in the valence band, thus the impurity band should only have a modest effect on the electrical conductivity when valence band conduction is strong.

5.2.2. Effect upon Seebeck—effective density of states mass

The density of states effective mass may be affected by an impurity band. The density of states may be changed by several high doping effects including the formation of impurity bands. Qualitatively a smear of the impurity band and valence band is expected. Thus, even though the conduction of impurity band is often only observable at low temperature, the Seebeck coefficient can be affected above room temperature. The details to calculate the transport coefficients can be found in Ref. [79]. The Seebeck coefficient is sensitive to the position of the Fermi level and how the density of states varies with energy. Both these factors can be affected

by an impurity band. There have been reports on change of density of states effective mass with varying doping concentration [53]. From a Pisarenko plot, one can find the density of states effective mass by fitting measured data. In Ref. [52], we obtained the best fitting by assuming an impurity band. Further, it was shown that camel-shaped curves of Seebeck coefficient with temperature, which is unusual in ZnSb, could be modelled by a temperature-dependent impurity band. It has been suggested that if one could engineer the energy structure of impurity band, then one could have a tool to enhance the thermoelectric performance [87].

Another impact of the impurity band may be on the *n*-type to *p*-type transition. This was suggested by Schneider by the observation of a sharp increase in the electrical conductivity on a temporary *n*-type and following *n*-type to *p*-type transition [71]. On a similar topic, though with different statements, Fedorov *et al.* rationalized the difficulty in doping ZnSb *n*-type by the formation of an impurity band close to the conduction band [21].

6. ZnSb synthesis techniques

Common synthesis methods for most of bulk thermoelectric materials can be categorized into three groups according to different processing steps, namely stoichiometric melts (SM), powder metallurgic method (PM), pseudo-pulverized and intermixed elements sintering method (Pseudo-PIES), as shown in **Figure 10**.

Polycrystalline ZnSb ingots can be synthesized by the so-called SM methods, i.e. melting of the elemental zinc and antimony followed by solidification in air or quenching in cold water. The purity of the starting elemental zinc and antimony materials has a significant impact on the resulting electrical properties. For example, starting materials with purities of 99.99% and 99.9999% allows to obtain the charge carrier concentration of $\sim 10^{19}$ and $\sim 10^{16} \text{ cm}^{-3}$, respectively, on undoped polycrystalline ZnSb [14]. Since ZnSb does not melt congruently, solidification will result in a mix of the phases, Zn_4Sb_3 , ZnSb and Sb. This mix can be homogenized by sufficient heat treatments to reach the thermodynamic equilibrium state with a single uniform ZnSb phase [14, 15]. Another problem with the solidification is that the sample contains cracks that significantly influence on the electron transport [13].

The solidified ingots are often milled into fine powder and pressed to pellets, which is a procedure that includes the basic ingredients of standard powder metallurgy (PM). Milling offers access to nanosized grains, thus providing possibility to enhance the thermoelectric properties. Earlier studies show that different milling techniques led to a trend of grain size as 80.0, 44.6 and 32.4 nm for manually grinding, dry-milling and wet-milling [16], as well as 10 nm for cryo-milling [88], respectively.

The PIES method (pulverized and intermixed elements sintering method) has been introduced into preparation of thermoelectric $(\text{Bi/Sb})_2(\text{Te/Se})_3$ materials, where all the elements are initially mixed and milled to fine powder before hot-pressing (no melting process) [89]. The electrical conductivity of the sample that was synthesized by this method has been reported about 5 times higher than that for the SM sample [90]. Distinguished from a typical PIES method, we often used pseudo-PIES for ZnSb, which partially mixed the dopant element with SM ingot in ball-milling, and then processed hot-pressing.

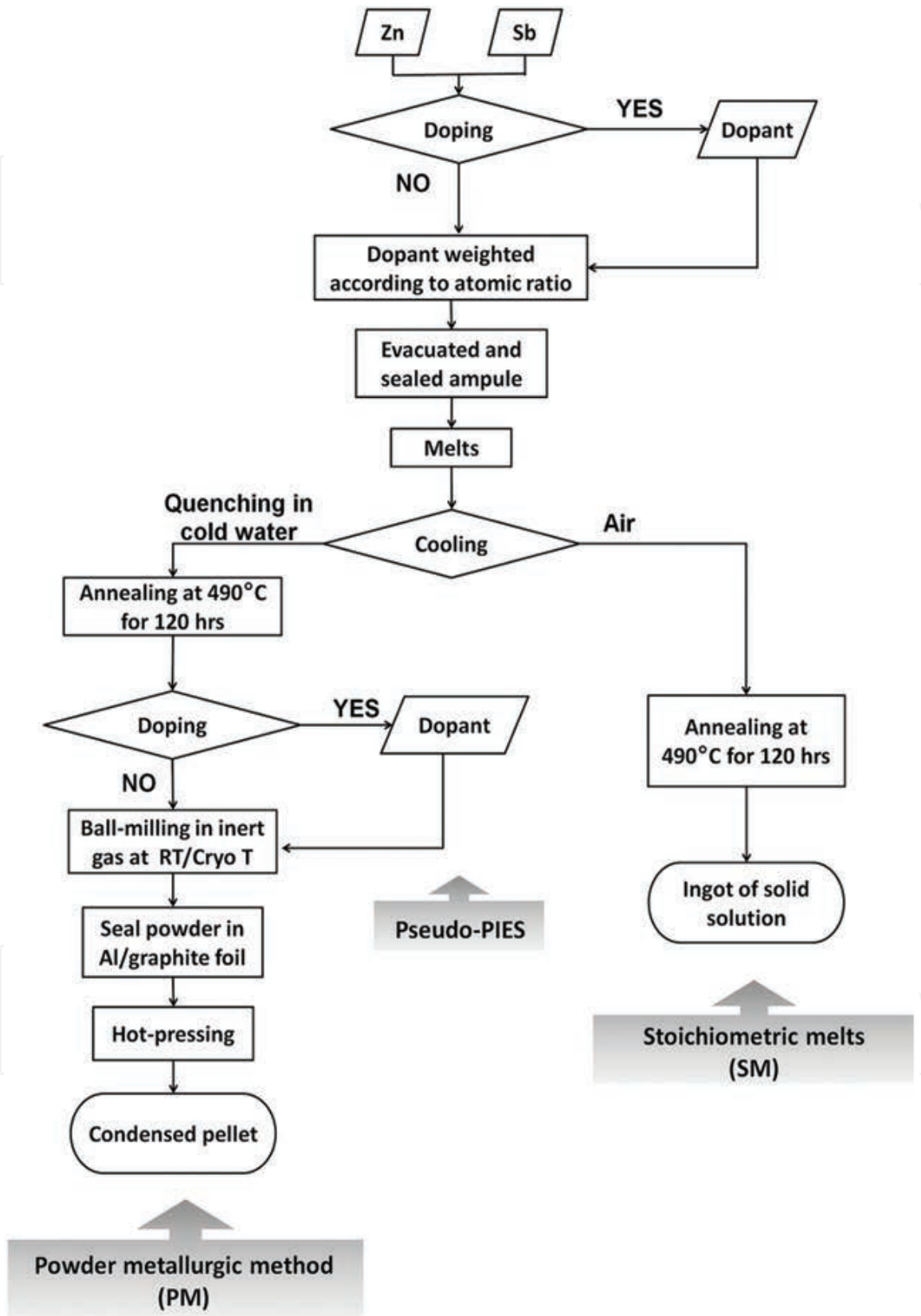


Figure 10. Flow chart of synthesis procedures. (Reprinted with author's permission from [29]. ©X. Song, 2016.)

There are different kinds of compaction techniques that follows powder metallurgy and have been used for fabrication of ZnSb samples. The most common ones are cold-pressing (at room temperature with ultra-pressure 2–10 GPa [83, 91]), hot-pressing (>450°C with pressure of 20–300 MPa [16, 19, 20, 35]), and spark plasma sintering (SPS) (the electrical current is passed through the sample with 5 min reaction time at 350–450°C [83, 92]). One important difference among hot-presses is the manipulation of secondary phases; both removal and proportioning are possible, and obviously depends upon the temperature and duration, but also on details of the instrument design and the environment of the ZnSb powder. Xiong *et al.* have reported that the volume fraction of Sb phase was estimated to be ~2 wt.% by Rietveld refinement in a hot-pressed sample [19] at 673 K in vacuum followed by an evacuated quartz ampoule and annealed at 673 K for 80 h. A recent study on SPS-samples showed also that Sb phase domains were distributed along the samples, accompanied with Zn₄Sb₃ on the surface [92]. Another difference is the final grain size of pellets. We have reported that rapid hot-press helped to minimize the grain size due to shorter cooling time [88].

Another important consideration of the synthesis technique is the ability to produce large amounts of thermoelectric materials in a cost-effective way. Considering that one of the favourable aspects of ZnSb from a commercial point of view is the low materials cost, there have been several efforts where the cost efficiency of the synthesis technique is important [92–94].

7. From laboratory to fabrication

ZnSb practical devices have been produced [9, 95], and there has been a promising achievement on thermoelectric performance of ZnSb in the laboratory. However, it is still challenging to transfer the achievement from laboratory to modern manufacturing. Progress in synthesis from different points of view have also to go through many tests regarding machinability, mechanical stability, thermal stability, thermal cycling and long-term stability, as well as compatibility with targeted fabrication techniques. Several of these issues are expected to contribute to—as well as benefit from—a further fundamental understanding of ZnSb, when practical solutions on short and long timescales are targeted. On a short to medium timescale, ZnSb can take advantage of new fabrication technologies that has been developed, but using traditional approaches for the device functionality. On a longer perspective, ZnSb may also be brought further into the explorations of new nanotechnology approaches to improve the performance of possible future generations of thermoelectrics.

One hindrance towards an ideal thermoelectric module made entirely of ZnSb is the inability to synthesis of stable *n*-type ZnSb. Although theoretical modelling shows favourable electronic structure of *n*-type ZnSb, there seems to be no promising paved routes to success. The direct synthesis of *n*-type ZnSb by doping would need a breakthrough. From an optimistic point of view that may arise indirectly from various other investigations on ZnSb, perhaps through defect engineering or a combination of different approaches, for example, modulation doping by embedded higher band gap materials with the appropriate band offsets for supply of electrons combined with compensation of Zn vacancy acceptors. A practical compromising

route towards module-making is using another semiconductor than ZnSb for the n -type leg, for instance $\text{Mg}_2\text{Sn}_{1-x}\text{Si}_x$ that matches ZnSb well in expected operation temperature, has the same environmentally friendly profile [20], as well as a low cost on raw materials. There might also be other suitable material candidates. Any practical problems with thermal expansion mismatch of materials in a module would have to be solved. Previous experiences with ZnSb modules have made it necessary to dope or add elements to ZnSb in order to achieve suitable mechanical properties. Fortunately, there has been a large development in packaging technology for electronic devices in the last couple of decades. New options for substrates and bonding techniques may be offered and meet the requirements on thermal expansion of the semiconductors.

The thermal stability of the synthesized ZnSb needs to be tested and probably be improved. This is one area where both fundamental studies and practical solutions may enter. ZnSb samples are subjected to Zn evaporation at high temperatures. The evaporation depends naturally very much on the ambient and the surface conditions. It is possible that protective layers can be applied to minimize evaporation. The situation has some similarities to that of several binary electronic materials, such as III–V materials, where one of the elements have a much higher vapour pressure, than what can be tolerated at the desired processing temperature. For GaAs, dielectric films SiO_2 and Si_3N_4 have been used for the purpose of preventing arsenic evaporation. A similar approach with a conformal deposition of a protective dielectric layer may be advantageous for ZnSb. Thermal stability also has to do with the thermal generation of point defects and their diffusion at elevated temperatures. The understanding of the phenomena is unsatisfactory from an academic point of view, in particular on the level of defect chemistry and electronic structure, but there are many experimental observations of the simple electrical parameters. Several authors have reported that after a heat treatment of ZnSb, the electrical conductivity and the charge carrier concentration increased, while the Seebeck coefficient decreased. The change was followed by a slow recovery towards the initial values at room temperature [15, 20, 44, 45, 47, 61, 77]. The characteristics can be related it to the $V_{\text{Zn}}\text{-Zn}_\text{I}$ Frenkel pair formation at elevated temperatures, and the recovery caused by their slower recombination at lower temperature. The vacancy concentration was linked to hole concentration. It was rationalized that these hysteresis effects would not be significant at high doping concentrations [15]. The doping effect on the vacancy concentration was then not considered. A detailed understanding of the vacancies, interstitials and their energy levels, ionization and formation energies is needed to understand the influence for higher doping concentration. The influence of more complicated defects can also be a large challenge. There are also reports on various temperature-cycling phenomena [52, 96, 97], involving the doping atoms and energy levels of these. Some of these effects may differ for different synthesis details.

The thermal stability is referring to all properties of the material, including the thermal conductivity. We have reported grain growth induced by heating, particularly in nanostructured bulk samples [88]. The grain growth will naturally induce a change of thermal conductivity due to the dependence on phonon scattering. To which extent, it constitutes a practical problem depends upon the targeted operation temperature. Approaches to minimize grain growth usually consist of adding atoms that segregate in grain boundaries, thereby preventing grain growth. This is an area that needs further study.

There are various routes that can make ZnSb a part of long-term exploration to improve thermoelectrics by nanostructures (not just nanograins). Some of them may use ways of depositing films of ZnSb, such as by MOCVD, sputtering [98, 99] and electroplating [11, 100], *etc.* By these techniques, it could be feasible to make composites and layered structures in a controlled way with different materials with suitable band offsets for energy filtering [101]. Possibilities of making high quality epitaxial films may also be attractive for fundamental material property studies. One might also do band engineering in the material by introducing misfit stress. Thin-film deposition may also offer a possibility to grow template nanostructures and exploiting the possibilities of quantum confinement in ZnSb and study the conduction band properties of ZnSb by injection into nanostructures.

Acknowledgements

The authors acknowledge support by the Norwegian Research Council under contract NFR11-40-6321 (NanoThermo) and the University of Oslo. The authors also thank to Dr. Patricia Almeida Carvalho for her contribution to transmission electron microscopic imaging.

Author details

Xin Song* and Terje G. Finstad

*Address all correspondence to: xins@fys.uio.no

Department of Physics, University of Oslo, Oslo, Norway

References

- [1] Seebeck, T.J., *Magnetische Polarisation der Metalle und Erze durch Temperatur Differenz*. A. J. v. Oettingen, 1823.
- [2] Berland, K., et al.: Enhancement of thermoelectric properties by energy filtering: Theoretical potential and experimental reality in nanostructured ZnSb. *Journal of Applied Physics*. 2016; **119**(12):125103.
- [3] Becquerel, E.: *Mempire sur les pouvoirs thermo-electriques des corps et sur les piles thermo-electroques*. *Annales de chimie et de physique*, 1866; **4**(8):389.
- [4] in *La Nature*. 1874. p. 19.
- [5] Halla F, Adler J.: *Röntgenographische Untersuchungen im System Cadmium-Antimon*. *Zeitschrift für anorganische und allgemeine Chemie*. 1929; **185**(1):184-192.

- [6] Halla, F, Nowotny H, Tompa H.: Röntgenographische Untersuchungen im System (Zn, Cd)–Sb.II. Zeitschrift für anorganische und allgemeine Chemie. 1933; **214**(2):196-200.
- [7] Olander A.: The Crystal Structure of CdSb. Zeitschrift für Kristallographie. 1935; **91**(3/4):243-247.
- [8] Almin KE.: The Crystal Structure of CdSb and ZnSb. Acta Chemica Scandinavica. 1948; **3**(3-4):400-407.
- [9] Telkes M.: Solar Thermoelectric Generators. Journal of Applied Physics. 1954; **25**(6):765-777.
- [10] Vedernikov MV, Iordanishvili EK. A.F. Ioffe and origin of modern semiconductor thermoelectric energy conversion. In: Proceedings of The XVII International Conference on Thermoelectrics (ICT 98); 1998. p. 37-42.
- [11] Saadat S, et al.: Template-Free Electrochemical Deposition of Interconnected ZnSb Nanoflakes for Li-Ion Battery Anodes. Chemistry of Materials. 2011; **23**(4):1032-1038.
- [12] Wang G, et al.: Investigation on pseudo-binary ZnSb-Sb₂Te₃ material for phase change memory application. Journal of Alloys and Compounds, 2015:341-346.
- [13] Miller RC. Survey of Known Thermoelectric Materials: ZnSb, In: Heikes RR, Ure Jr. RW, editors. Thermoelectricity: Science and engineering. New York: Interscience Publishers; 1961. p. 405.
- [14] Justi E, Rasch W, Schneider G.: Untersuchungen an zonengeschmolzenen ZnSb-einkristallen. Advanced Energy Conversion. 1964; **4**(1):27-38.
- [15] Shaver PJ, Blair J.: Thermal and Electronic Transport Properties of p-Type ZnSb. Physical Review. 1966; **141**(2):649-663.
- [16] Böttger PHM, et al.: Influence of Ball-Milling, Nanostructuring, and Ag Inclusions on Thermoelectric Properties of ZnSb. Journal of Electronic Materials, 2010. **39**(9): p. 1583-1588.
- [17] Okamura C, Ueda T, Hasezaki K.: Preparation of Single-Phase ZnSb Thermoelectric Materials Using a Mechanical Grinding Process. Materials Transactions. 2010; **51**(5): 860-862.
- [18] Valset K, et al.: Thermoelectric properties of Cu doped ZnSb containing Zn₃P₂ particles. Journal of Applied Physics. 2012; **111**(2):023703.
- [19] Xiong D-B, Okamoto NL, Inui H.: Enhanced thermoelectric figure of merit in p-type Ag-doped ZnSb nanostructured with Ag₃Sb. Scripta Materialia. 2013; **69**(5):397-400.
- [20] Fedorov MI, et al.: New Interest in Intermetallic Compound ZnSb. Journal of Electronic Materials. 2014; **43**(6):2314-2319.
- [21] Fedorov MI, et al.: Thermoelectric efficiency of intermetallic compound ZnSb. Semiconductors. 2014; **48**(4):432-437.
- [22] Valset K, Song X, Finstad TG. Stability and thermoelectric properties of Cu doped ZnSb. In: Proceedings of The European Conference on Thermoelectrics (ECT 2014); 2014. Madrid, Spain.

- [23] Guo Q, Luo S.: Improved thermoelectric efficiency in p-type ZnSb through Zn deficiency. *Functional Materials Letters*. 2015; **08**(02):1550028.
- [24] Valset K. A Technique to Measure Thermoelectric Figure of Merit and Heat Flow at High Temperatures by Cancelling Heat Losses. In: *Proceedings of The 12th European Conference on Thermoelectrics; Materials Today*. 2015; **2**(2):721-728.
- [25] Carter FL, Mazelsky R.: The ZnSb structure; A further enquiry. *Journal of Physics and Chemistry of Solids*. 1964; **25**(6):571-581.
- [26] Mikhaylushkin AS, Nylén J, Häussermann U.: Structure and Bonding of Zinc Antimonides: Complex Frameworks and Narrow Band Gaps. *Chemistry – A European Journal*. 2005; **11**(17):4912-4920.
- [27] Mozharivskiy Y, et al.: A Promising Thermoelectric Material: Zn_4Sb_3 or $Zn_{6-\delta}Sb_5$. Its Composition, Structure, Stability, and Polymorphs. *Structure and Stability of $Zn_{1-\delta}Sb$* . *Chemistry of Materials*. 2004; **16**(8):1580-1589.
- [28] Toman K.: On the structure of ZnSb. *Journal of Physics and Chemistry of Solids*. 1960; **16**(1): 160-161.
- [29] Song X. Thermoelectric Transport and Microstructure of ZnSb, In: *Department of Physics*. 2016, University of Oslo: Oslo, Norway. p. 138.
- [30] Mooser E, Pearson WB.: Chemical Bond in Semiconductors. *Physical Review*. 1956; **101**(5): 1608-1609.
- [31] Häussermann U, Mikhaylushkin AS.: Electron-poor antimonides: complex framework structures with narrow band gaps and low thermal conductivity. *Dalton Transactions*. 2010. **39**(4):1036-1045.
- [32] Arushanov EK.: Crystal growth, characterization and application of II-V compounds. *Progress in Crystal Growth and Characterization*. 1986. **13**(1):1-38.
- [33] Justi E, Lautz G.: Über die Störstellen- und Eigenhalbleitung intermetallischer Verbindungen. In: *Zeitschrift für Naturforschung A*. 1952. p. 191.
- [34] Velický B, Frei V.: The chemical bond in CdSb. *Czechoslovakij fiziceskij zurnal B*. 1963; **13**(8):594-598.
- [35] Fischer A, et al.: Synthesis, Structure, and Properties of the Electron-Poor II-V Semiconductor ZnAs. *Inorganic Chemistry*. 2014; **53**(16):8691-8699.
- [36] Niedziolka K, et al.: Theoretical and experimental search for ZnSb-based thermoelectric materials. *Journal of Physics: Condensed Matter*, 2014; **26**(36):365401.
- [37] Niedziółka K, Jund P.: Influence of the Exchange-Correlation Functional on the Electronic Properties of ZnSb as a Promising Thermoelectric Material. *Journal of Electronic Materials*. 2015; **44**(6):1540-1546.
- [38] Benson D, Sankey OF, Häussermann U.: Electronic structure and chemical bonding of the electron-poor II-V semiconductors ZnSb and ZnAs. *Physical Review B*. 2011; **84**(12):125211.

- [39] Böttger PHM, et al.: Electronic structure of thermoelectric Zn-Sb. *Journal of Physics: Condensed Matter*. 2011; **23**(26):265502.
- [40] Bjerg L, Madsen GKH, Iversen BB.: Enhanced Thermoelectric Properties in Zinc Antimonides. *Chemistry of Materials* 2011; **23**(17):3907-3914.
- [41] Zhao J-H, et al.: First Principles Study on the Electronic Properties of $Zn_{64}Sb_{64-x}Te_x$ Solid Solution ($x = 0, 2, 3, 4$). *International Journal of Molecular Sciences*. 2011; **12**(5):3162-3169.
- [42] Jund P, et al.: Physical properties of thermoelectric zinc antimonide using first-principles calculations. *Physical Review B*. 2012; **85**(22):224105.
- [43] Yamada Y.: Band structure calculation of ZnSb. *physica status solidi (b)*. 1978; **85**(2):723-732.
- [44] Turner WJ, Fischler AS, Reese WE.: Physical Properties of Several II-V Semiconductors. *Physical Review*. 1961; **121**(3):759-767.
- [45] Komiya H, Masumoto K, Fan HY.: Optical and Electrical Properties and Energy Band Structure of ZnSb. *Physical Review*. 1964; **133**(6A):A1679-A1684.
- [46] Eisner RL, Mazelsky R, Tiller WA.: Growth of ZnSb Single Crystals. *Journal of Applied Physics* 1961; **32**(10):1833-1834.
- [47] Kostur NL, Psarev VI.: Electrical properties of doped single crystals of ZnSb. *Soviet Physics Journal*. 1967; **10**(2):21-23.
- [48] Zhang LT, et al.: Effects of ZnSb and Zn inclusions on the thermoelectric properties of β - Zn_4Sb_3 . *Journal of Alloys and Compounds*. 2003; **358**(1-2):252-256.
- [49] Goldsmid HJ, Sharp JW.: Estimation of the thermal band gap of a semiconductor from Seebeck measurements. *Journal of Electronic Materials*. 1999; **28**(7):869-872.
- [50] Schmitt J, et al.: Resolving the true band gap of ZrNiSn half-Heusler thermoelectric materials. *Materials Horizons*. 2015; **2**(1):68-75.
- [51] Gibbs ZM, et al.: Band gap estimation from temperature dependent Seebeck measurement-Deviations from the $2e|S|_{\max}T_{\max}$ relation. *Applied Physics Letters*. 2015; **106**(2):022112.
- [52] Valsert K, Song X, Finstad TG.: A study of transport properties in Cu and P doped ZnSb. *Journal of Applied Physics*. 2015; **117**(4):045709.
- [53] Böttger PHM, et al.: Doping of p-type ZnSb: Single parabolic band model and impurity band conduction. *physica status solidi (a)*. 2011; **208**(12):2753-2759.
- [54] Van Overstraeten RJ, Mertens RP.: Heavy doping effects in silicon. *Solid-State Electronics*. 1987; **30**(11):1077-1087.
- [55] Toberer ES, et al.: Traversing the Metal-Insulator Transition in a Zintl Phase: Rational Enhancement of Thermoelectric Efficiency in $Yb_{14}Mn_{1-x}Al_xSb_{11}$. *Advanced Functional Materials*. 2008; **18**(18):2795-2800.

- [56] May AF, et al.: Characterization and analysis of thermoelectric transport in n-type $\text{Ba}_8\text{Ga}_{16-x}\text{Ge}_{30+x}$. *Physical Review B*. 2009; **80**(12):125205.
- [57] Toberer ES, May AF, Snyder GJ.: *Zintl Chemistry for Designing High Efficiency Thermoelectric Materials*. *Chemistry of Materials*. 2010; **22**(3):624-634.
- [58] Mlnařiková L, Tříška A, Štourač L.: The transport phenomena of pure and doped p-type ZnSb. *Czechoslovak Journal of Physics B*. 1970; **20**(1):63-72.
- [59] Stevenson MJ, Cyclotron Resonance in II-V Semiconductors. In: *Proceedings of The International Conference on Semiconductor Physics*. 1961. Prague: Czechoslovakian Academy of Science.
- [60] Telkes M.: The Efficiency of Thermoelectric Generators. I. *Journal of Applied Physics*. 1947; **18**(12):1116-1127.
- [61] Kot MV, Kretsu IV.: Anisotropy of certain electrical properties of single crystals of Zinc Antimony. *Fiz.Tverd.Tela*. 1960; 2:1250 (*Soviet Physics-Solid State*. 1960; 2:1134).
- [62] Hrubý A, Beránková J, Míšková V.: Growth of ZnSb Single Crystals. *physica status solidi (b)*. 1963; **3**(2):289-293.
- [63] Závětová M.: Absorption Edge of ZnSb. *physica status solidi (b)*. 1964; **5**(1):K19-K21.
- [64] Prokofieva LV, et al.: Doping and defect formation in thermoelectric ZnSb doped with copper. *Semiconductors*. 2014; **48**(12):1571-1580.
- [65] Ridley BK. *Quantum Processes in Semiconductors*. 4th ed. Oxford: Oxford Science Publications; 1999.
- [66] Goldsmid HJ. *Introduction to Thermoelectricity*. Oxford: Oxford University Press; 2009.
- [67] Ito M, Ohishi Y, Muta H, Kurosaki K, Yamanaka S.: Thermoelectric properties of Zn-Sn-Sb based alloys. In: *MRS Proceedings Symposium LL – Thermoelectric Materials for Solid-State Power Generation and Refrigeration*. 2011.
- [68] Prokofieva LV, Konstantinov PP, Shabal'din AA.: On the tin impurity in the thermoelectric compound ZnSb: Charge-carrier generation and compensation. *Semiconductors*. 2016; **50** (6): 741-750.
- [69] Sottmann J, et al.: Synthesis and Measurement of the Thermoelectric Properties of Multiphase Composites: ZnSb Matrix with Zn_4Sb_3 , Zn_3P_2 , and Cu_5Zn_8 . *Journal of Electronic Materials*. 2013; **42**(7):1820-1826.
- [70] Šmirous K, Hrubý A, Štourač L.: The influence of impurities on the electric and thermoelectric properties of CdSb single crystals. *Czechoslovakij fiziceskij zurnal B*. 1963; **13** (5):350-357.
- [71] Schneider G.: Preparation and Properties of n-Type ZnSb. *physica status solidi (b)*. 1969; **33**(2):K133-K136.

- [72] Zeid AA, Schneider G.: Various Donors in n-ZnSb and the Influence of Sample Treatment. *Zeitschrift für Naturforschung A*. 1975; **30**(3):381.
- [73] Ueda T, et al.: Effect of Tellurium Doping on the Thermoelectric Properties of ZnSb. *Journal of the Japan Institute of Metals and Materials*. 2010; **74**(2):110-113.
- [74] Bjerg L, Madsen GKH, Iversen BB.: Ab initio Calculations of Intrinsic Point Defects in ZnSb. *Chemistry of Materials*. 2012; **24**(11):2111-2116.
- [75] Silvey GA, Lyons VJ, Silvestri VJ.: The Preparation and Properties of Some II – V Semiconducting Compounds. *Journal of The Electrochemical Society*. 1961; **108**(7):653-658.
- [76] Campbell SA. *The Science and Engineering of Microelectronic Fabrication*. Oxford: University Press; 1996.
- [77] Kretsu IV, Kot MV.: Thermal Dissociation of Cadmium and Zinc Antimonide Crystals. *Uchenye Zapiski Kazanskogo Universiteta (Proceedings of Kazan University)*, 1961; **49**: 105-111.
- [78] Singleton J, ed. *Band Theory and Electronic Properties of Solids*. Oxford Master Series in Condensed Matter Physics. 2001.
- [79] Song X, et al.: Impurity band conduction in the thermoelectric material ZnSb. *Physica Scripta*. 2012; **2012**(T148):014001.
- [80] Hung CS.: Theory of Resistivity and Hall Effect at Very Low Temperatures. *Physical Review*. 1950; **79**(4):727-728.
- [81] Hung CS, Gliessman JR.: The Resistivity and Hall Effect of Germanium at Low Temperatures. *Physical Review*. 1950; **79**(4):726-727.
- [82] Hung CS, Gliessman JR.: Resistivity and Hall Effect of Germanium at Low Temperatures. *Physical Review*. 1954; **96**(5):1226-1236.
- [83] Eklof D, et al.: Transport properties of the II-V semiconductor ZnSb. *Journal of Materials Chemistry A*. 2013; **1**(4):1407-1414.
- [84] Schubert EF. *Physical Foundations of Solid-State Devices*. 2006.
- [85] James HM, Ginzburg AS.: Band Structure in Disordered Alloys and Impurity Semiconductors. *The Journal of Physical Chemistry*. 1953; **57**(8):840-848.
- [86] Rawat PK, Paul B, Banerji P.: Impurity-band induced transport phenomenon and thermoelectric properties in Yb doped $\text{PbTe}_{1-x}\text{I}_x$. *Physical Chemistry Chemical Physics*. 2013; **15**(39):16686-16692.
- [87] Goldsmid HJ.: Impurity Band Effects in Thermoelectric Materials. *Journal of Electronic Materials*. 2012; **41**(8):2126-2129.
- [88] Song X, et al.: Nanostructuring of Undoped ZnSb by Cryo-Milling. *Journal of Electronic Materials*. 2015; **44**(8):2578-2584.

- [89] Ohta T, et al.: Pulverized and Intermixed Elements Sintering Method for (Bi, Sb)₂(Te, Se)₃ based n-type Thermoelectric Devices. *IEEJ Transactions on Power and Energy*. 1991; **111** (6): 670-674.
- [90] Toshitaka O, Takenobu K.: PIES Method of Preparing Bismuth Alloys, In: *CRC Handbook of Thermoelectrics*. CRC Press; 1995.
- [91] Zhao WY, Wang Y, Zhai P, Tang X, Zhang Q.: Method for forming ZnSb-based block thermoelectric material at ultra-high pressure and cold pressure. 2007, Google Patents.
- [92] Blichfeld AB, Iversen BB.: Fast direct synthesis and compaction of phase pure thermoelectric ZnSb. *Journal of Materials Chemistry C*. 2015; **3**(40):10543-10553.
- [93] Lee HB, et al.: Thermoelectric properties of screen-printed ZnSb film. *Thin Solid Films*. 2011; **519**(16):5441-5443.
- [94] Pothin R, et al.: Preparation and properties of ZnSb thermoelectric material through mechanical-alloying and Spark Plasma Sintering. *Chemical Engineering Journal*. 2016; **299**: 126-134.
- [95] Farmer M.G. Improvement in thermo-electric batteries. 1870, Google Patents.
- [96] Shabaldin AA, et al.: The Influence of Weak Tin Doping on the Thermoelectric Properties of Zinc Antimonide. *Journal of Electronic Materials*, 2016. **45**(3): p. 1871-1874.
- [97] Shabaldin AA, et al.: Acceptor Impurity of Copper in ZnSb Thermoelectric. *Materials Today: Proceedings of The 12th European Conference on Thermoelectrics*. 2015; **2**(2):699-704.
- [98] Fan P, et al.: Thermoelectric properties of zinc antimonide thin film deposited on flexible polyimide substrate by RF magnetron sputtering. *Journal of Materials Science: Materials in Electronics*. 2014; **25**(11):5060-5065.
- [99] Zheng Z-H, et al.: Enhanced thermoelectric properties of Cu doped ZnSb based thin films. *Journal of Alloys and Compounds*. 2016; **668**:8-12.
- [100] Mann O, Freyland W.: Mechanism of formation and electronic structure of semiconducting ZnSb nanoclusters electrodeposited from an ionic liquid. *Electrochimica Acta*. 2007; **53**(2):518-524.
- [101] Flage-Larsen EL, Martin O. Band structure guidelines for higher figure-of-merit; analytic band generation and energy filtering. In: Rowe DM, editor. *Thermoelectrics and its Energy Harvesting: Materials, Preparation, and Characterization in Thermoelectrics*. CRC Press; 2012.

